galaxies

MDPI

Article

Implications of the Intriguing Constant Inner Mass Surface Density Observed in Dark Matter Halos

Jorge Sánchez Almeida [1,2]

[1] Instituto de Astrofísica de Canarias, 38200 La Laguna, Tenerife, Spain; jos@iac.es
[2] Departamento de Astrofísica, Universidad de La Laguna, 38200 La Laguna, Tenerife, Spain

Abstract: It has long been known that the observed mass surface density of cored dark matter (DM) halos is approximately constant, independently of the galaxy mass (i.e., $\rho_c r_c \simeq$ constant, with ρ_c and r_c being the central volume density and the radius of the core, respectively). Here, we review the evidence supporting this empirical fact as well as its theoretical interpretation. It seems to be an emergent law resulting from the concentration–halo mass relation predicted by the current cosmological model, where the DM is made of collisionless cold DM particles (CDM). We argue that the prediction $\rho_c r_c \simeq$ constant is not specific to this particular model of DM but holds for any other DM model (e.g., self-interacting) or process (e.g., stellar or AGN feedback) that redistributes the DM within halos conserving its CDM mass. In addition, the fact that $\rho_c r_c \simeq$ constant is shown to allow the estimate of the core DM mass and baryon fraction from stellar photometry alone is particularly useful when the observationally expensive conventional spectroscopic techniques are unfeasible.

Keywords: dark matter; dark matter cores; fundamental parameters; halos; stellar distribution

1. Introduction

The shape of the dark matter (DM) halos hosting galaxies can be inferred from rotation curves or other kinematical measurements, e.g., [1–3]. The resulting DM radial profiles often show an inner plateau or *core* characterized by a central mass density ρ_c and a core radius r_c which, when combined, happen to yield a surface density approximately constant,

$$\rho_c r_c \simeq \text{constant}, \tag{1}$$

a property observed to hold in a wide range of halo masses M_h, between 10^9 and $10^{12}\,M_\odot$ [4–12] (actual values and details will be given in Section 2 and Appendix A). Originally, it was a rather surprising result [4], but currently it is interpreted in the literature as an emergent law caused by the well-known relation between halo mass and concentration arising in collisionless cold dark matter (CDM) numerical simulations [13–15]. In CDM-only simulations, the CDM halos do not have cores. They follow the canonical NFW profiles [16] or the Einasto profiles [17], with a pronounced inner cusp where the density grows continuously toward the center of the halo. Thus, an additional physical process must operate to transform the cuspy CDM halos into cored halos, conserving the original DM mass. This transformation is usually assumed to be driven by baryon processes like star-formation feedback, AGN feedback, or galaxy mergers, which shuffle around the baryonic mass, thus changing the overall gravitational potential and affecting the distribution of CDM. CDM cores appear in model galaxies formed in full hydrodynamical cosmological numerical simulations, e.g., [18–20]. Thus, Equation (1) is often regarded as a support for

check for updates

Academic Editor: Jose Gaite

Received: 22 November 2024
Revised: 28 December 2024
Accepted: 7 January 2025
Published: 9 January 2025

Citation: Sánchez Almeida, J. Implications of the Intriguing Constant Inner Mass Surface Density Observed in Dark Matter Halos. *Galaxies* **2025**, *13*, 6. https://doi.org/10.3390/galaxies13010006

Copyright: © 2025 by the author. Licensee MDPI, Basel, Switzerland. This article is an open access article distributed under the terms and conditions of the Creative Commons Attribution (CC BY) license (https://creativecommons.org/licenses/by/4.0/).

CDM; [15] and references therein. However, the formation of cores in DM halos can be driven by any physical process that thermalizes the DM distribution [21,22]. They will also render Equation (1), provided the process just redistributes the available mass, not much changing the relation between the halo mass and concentration set by the cosmological initial conditions (Section 5.1).

The purpose of this work is to review the observational evidence for Equation (1) as well as the theory behind it. The interpretation can be pinned down to the relation between the mass of a DM halo and its age of formation (Section 5.1), which is set by cosmology and to a lesser extent by details on the nature of DM. As a spin-off, we demonstrate how Equation (1) can be used to estimate the mass in the DM halo of a galaxy based solely on the distribution of its stars. The approach is based on the fact that dwarf galaxies also tend to show a central plateau or core in the stellar distribution, e.g., [23,24]. The radii of the stellar and the DM cores are expected to scale with each other [25,26]. We worked out the relation between the core radius of the stellar distribution and the DM mass.

The paper is organized as follows: Section 2 collects observational evidence for Equation (1). Section 3 works out the explanation of Equation (1) within CDM. Section 4 compares the observations in Section 2 with the theory in Section 3. Based on Equation (4), Section 5 writes down a semi-empirical relation between the stellar core radius and DM halo mass. It also shows that the stellar mass surface density is a proxy for the baryon fraction in the center of a galaxy. Ready-to-use relations are given in Equations (25) and (26). Section 6 summarizes the main conclusions in the work.

2. Observations Supporting Equation (1)

As we point out in Section 1, the product $\rho_c r_c$ is approximately constant over a large range in galaxy mass. To emphasize the existing evidence, we have compiled a number of relations between $\rho_c r_c$ and M_h from the literature. They are based on uneven measurements prone to bias, including the determination of the DM halo mass of a galaxy and the definition of core radius. However, the conclusion is clear, with the different independent determinations agreeing within error bars. The result of the compilation is shown in Figures 1–5. Details of how the individual works were interpreted to construct the figures are given in Appendix A. In particular, here and throughout the paper, we assume the core radius to be the radius where the density drops to half the central value,

$$\rho(r_c) = \rho_c/2, \tag{2}$$

with $\rho_c = \rho(0)$. This definition is not universally used and so the radii quoted in the original reference often have to be transformed to our definition, as detailed in Appendix A.

Figure 1 gives the scatter plot of $\rho_c r_c$ versus M_h. The extreme values are likely unreliable but it is clear that the product $\rho_c r_c$ tends to be constant, at least for $M_h < 10^{11} M_\odot$. This fact is better appreciated in Figure A1, which is identical to Figure 1 but with the vertical axis spanning the same eight orders of magnitude of the horizontal axis corresponding to the DM halo masses. Histograms with the values of $\rho_c r_c$ in Figure 1 are shown in Figure 2. They include all the observed values (the blue line), when $M_h < 10^{12} M_\odot$ (the red line), and when $M_h < 10^{11} M_\odot$ (the green line). An inset in the figure also gives the median and the 1-sigma percentiles of the distributions (i.e., 50 %, 15.9 %, and 84.1 %) which correspond to

$$\rho_c r_c = 44^{+44}_{-21}\, M_\odot\, \mathrm{pc}^{-2}, \tag{3}$$

when $M_h < 10^{11} M_\odot$, a limit representative of dwarf galaxies. We note that the used r_c, as set by Equation (2), is typically a factor of two smaller than the core radii commonly defined in the literature (e.g., b when the Schuster–Plummer profile in Equation (5) is used). Thus, the surface density in Equation (3) is fully consistent with a value around 100 $M_\odot$ pc^{-2} often quoted in the literature (see, e.g., [5,14]). As we explain in Appendix A, the estimate of M_h used in Figure 1 relies on the observed absolute magnitude of the galaxies, assuming a mass-to-light ratio and a relation between stellar mass and DM halo mass as inferred from abundance matching [27]. However, the trend for $\rho_c r_c$ to become constant in dwarf galaxies is already present in the original data; see Figure 3, where the abscissa are given by the measured absolute magnitude of the galaxy.

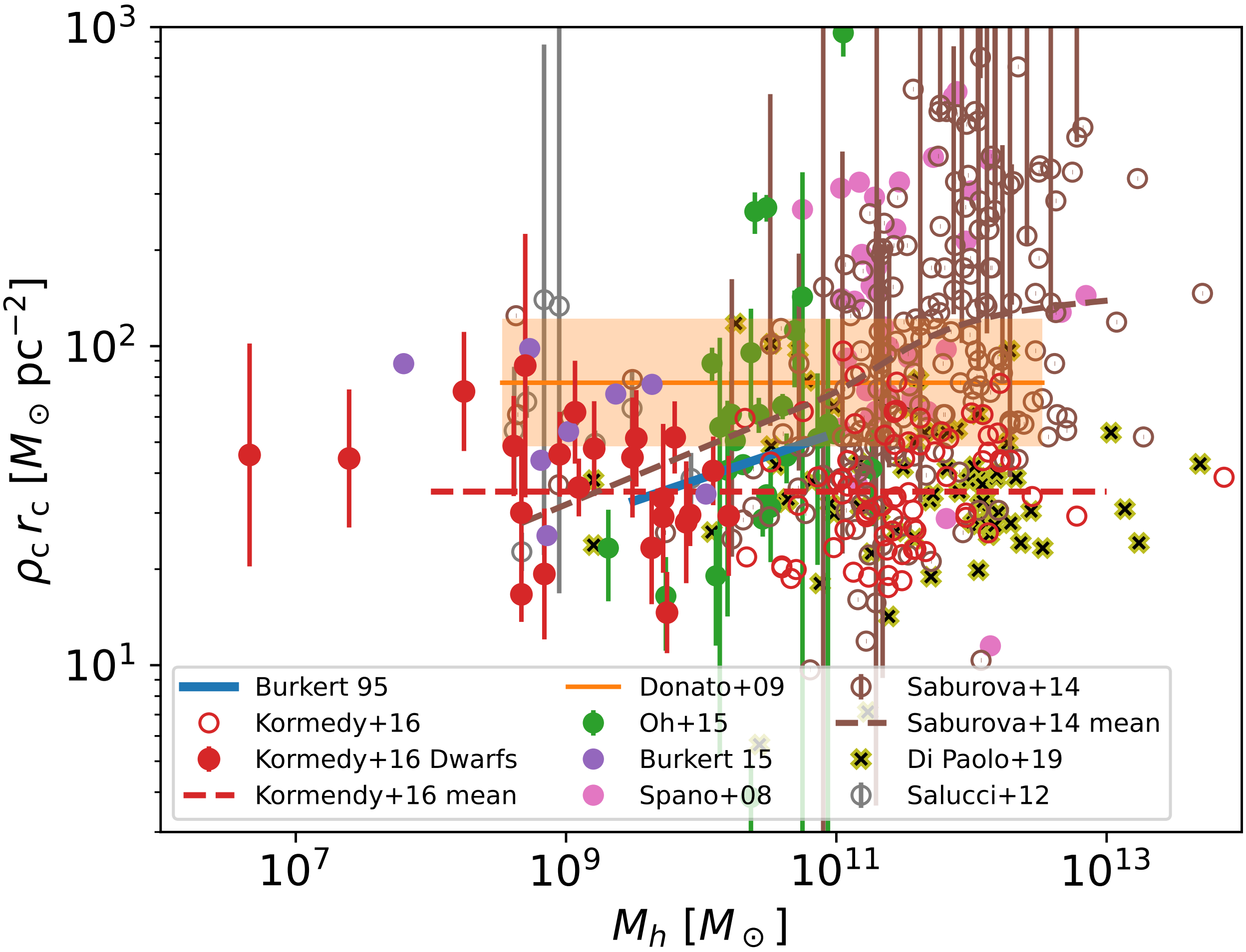

Figure 1. Compilation of values of $\rho_c r_c$ from the literature as a function of the DM halo mass of the galaxy (M_h). Details on the references and the processing are given in Appendix A. A version of this figure, but showing the same eight orders of magnitude range for abscissae and ordinates, is shown in Figure A1. References: Burkert 95 [4], Kormendy+16 [11], Donato+09 [7], Oh+15 [2], Burkert 15 [10], Spano+08 [6], Saburova+14 [9], Di Paolo+19 [12], and Salucci+12 [8]. The inset gives a color and symbol code which is the same used in Figures 3–5.

Figure 4 gives $\rho_c r_c$ (top panel) and $\rho_c r_c^3$ (bottom panel) versus r_c. Note that the latter gives the DM mass in the core and it scales as r_c^2 following Equation (3), which is represented in the figure by the gray dashed line. These relations are independent of the uncertainties in M_h.

Figure 5 gives the relation of r_c with M_h (top panel) and ρ_c with M_h (bottom panel). The correlation happens to be very clear in both cases. The larger the mass, the larger the radius and the smaller the density. In order to guide the eye, the figure includes power laws as $r_c \propto M_h^{0.4}$ (top panel) and $\rho_c \propto M_h^{-0.4}$ (bottom panel), which approximately describe the observed trends. Note that combined, these power laws render Equation (1).

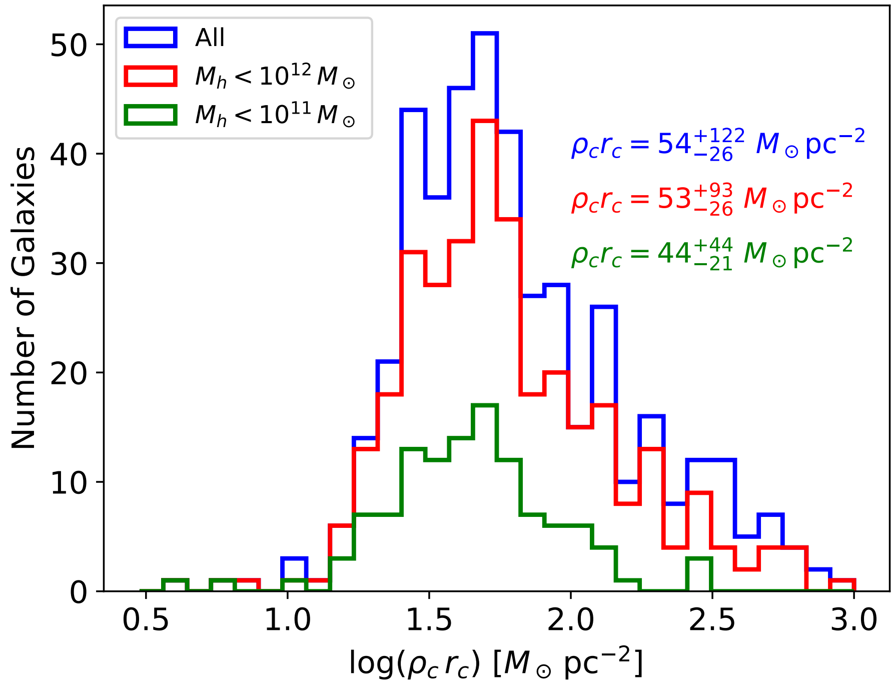

Figure 2. Histograms with the distribution of $\rho_c r_c$ represented in Figure 1 and detailed in Appendix A. We show three different selections: all galaxies (the blue line), galaxies with halo masses $M_h < 10^{12}\,M_\odot$ (the red line), and galaxies with $M_h < 10^{11}\,M_\odot$ (the green line). The last one is representative of dwarf galaxies. The inset gives the median of each distribution, as well as the range between percentiles 15.9 % and 84.1 % (i.e., median ± 1 sigma).

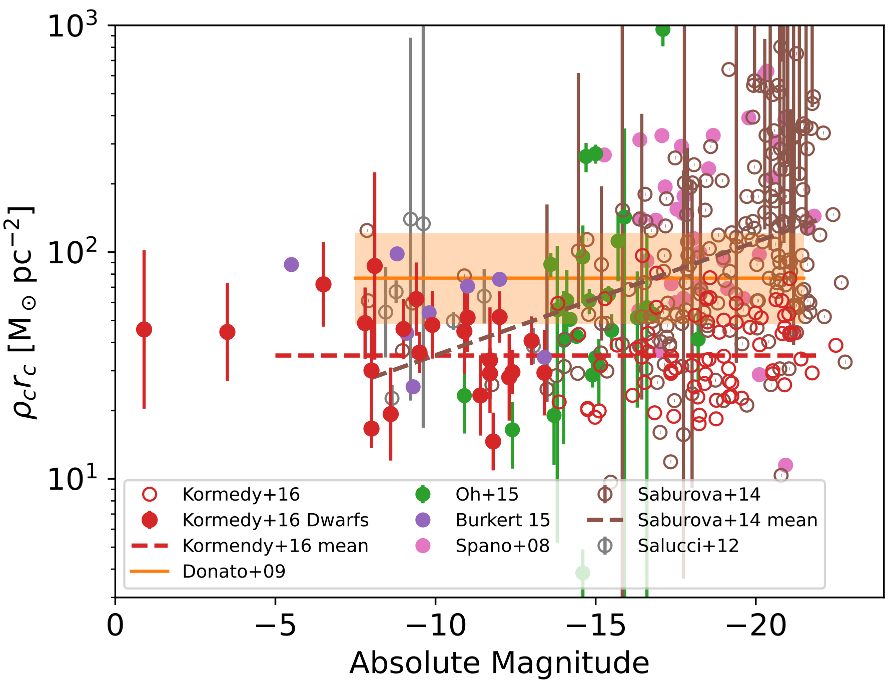

Figure 3. Central DM surface density, $\rho_c r_c$, as a function of the absolute magnitude of the galaxy, which is the observable employed to estimate the halo masses represented in Figure 1. The absolute magnitude is M_B or M_V depending on the galaxy. The inset gives the color and symbol code, which is the same employed in Figures 1, 4 and 5.

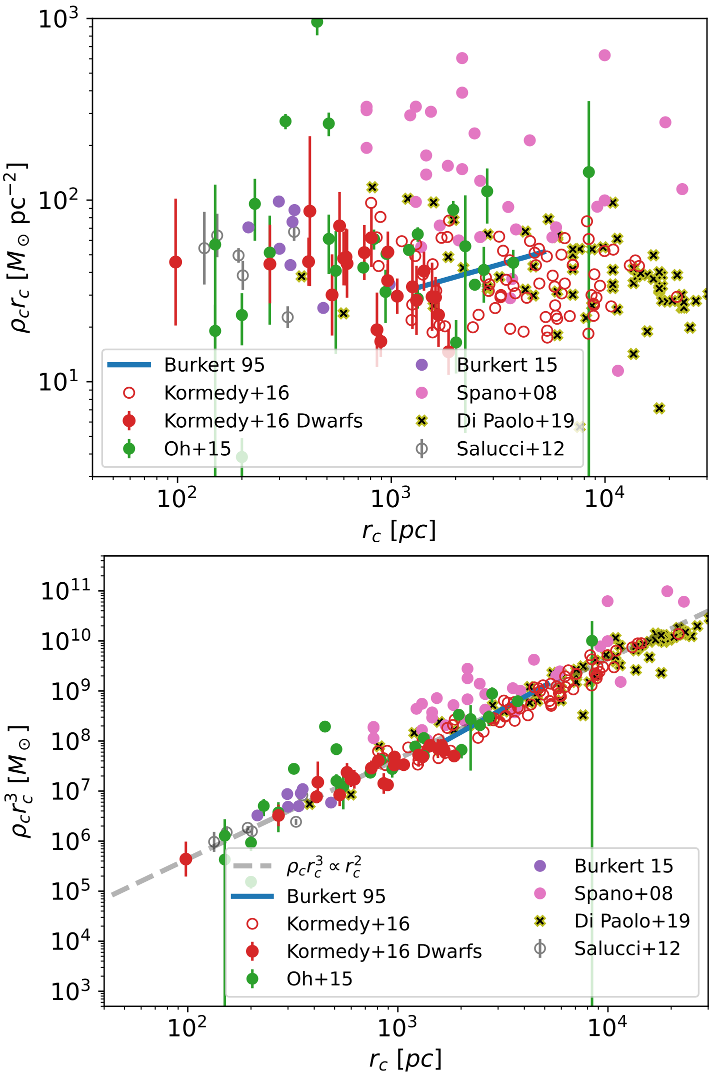

Figure 4. Observed $\rho_c r_c$ versus r_c (**top panel**) and $\rho_c r_c^3$ versus r_c (**bottom panel**). Note that the latter gives the DM mass in the core and scales as r_c^2 following Equation (3), which is represented by the gray dashed line. These relations do not depend on the total DM halo mass and can be used to test theoretical explanations bypassing uncertainties in M_h. The insets give the color and symbol code, used also in Figures 1, 3 and 5.

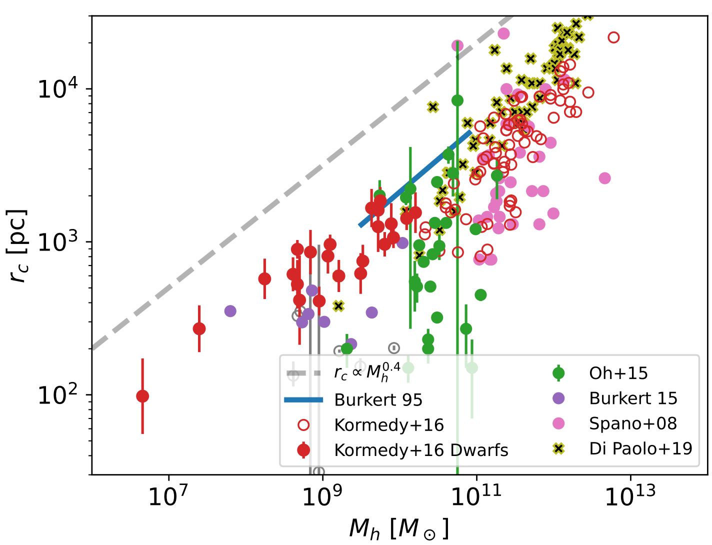

Figure 5. *Cont.*

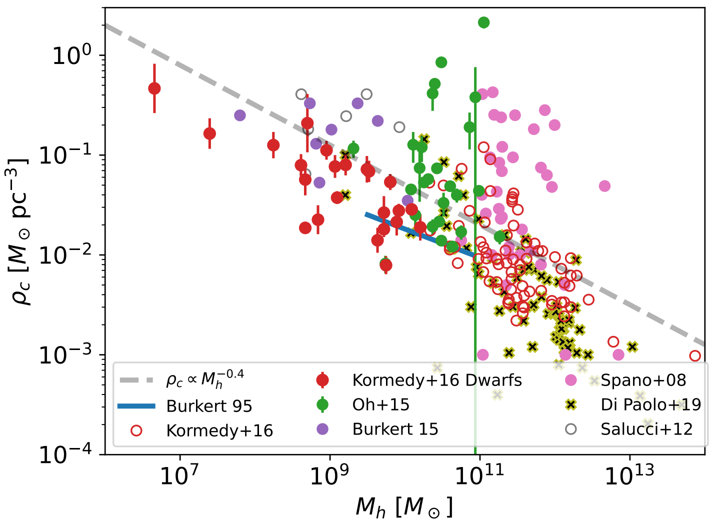

Figure 5. (**Top panel**): core radius r_c versus DM halo mass M_h. The dashed line is a power law with exponent $+0.4$ and has been included to guide the eye. (**Bottom panel**): central DM density ρ_c versus DM halo mass. This time, the dashed line is a power law with exponent -0.4. The insets give the color and symbol code, which is the same used in Figures 1, 3 and 4.

3. Theory: Cores Resulting from Redistributing Collisionless Cold Dark Matter Halos

If the DM was collisionless CDM and if there were no baryons, then the distribution of DM within each halo would approximately follow the iconic NFW profile [16],

$$\rho_{\rm NFW}(r) = \frac{\rho_s}{(r/r_s)\,(1 + r/r_s)^2}, \tag{4}$$

describing the variation with radius r of the DM volume density $\rho_{\rm NFW}(r)$. The parameters r_s and ρ_s stand for a scaling radius and a scaling density, respectively. The mass available to form any DM halo today is provided by the initial conditions set by cosmology (see Section 5.1). It would be the same independently of whether a physical process redistributes this mass in a different mass density profile. Probably, the most general of such a process is the thermalization the DM distribution. In this case, one expects the formation of a core with a generic polytropic shape, characteristic of self-gravitating systems reaching thermodynamic equilibrium [21,22,28]. For analytic simplicity, we assume $m = 5$ polytrope (best known as the Schuster–Plummer profile), but the core of all the polytropes has virtually the same shape, e.g., [28]. In this case,

$$\rho_5(r) = \frac{\rho_c}{[1 + (r/b)^2]^{5/2}}, \tag{5}$$

with ρ_c the central density and b a length scale setting the core radius defined as in Equation (1),

$$r_c = b \times \sqrt{2^{2/5} - 1} \simeq b \times 0.56525\ldots. \tag{6}$$

Thus, the new density profile resulting from the core formation is a piecewise function defined as Equation (5) in the core, Equation (4) in the outskirts, and continuous in the matching radius r_m,

$$\rho(r) = \begin{cases} \rho_5(r), & \text{when } r < r_m, \\ \rho_5(r_m) = \rho_{\rm NFW}(r_m), & \text{when } r = r_m, \\ \rho_{\rm NFW}(r), & \text{when } r > r_m. \end{cases} \tag{7}$$

In addition, to conserve mass,

$$\int_0^\infty \rho(r)\, r^2\, dr = \int_0^\infty \rho_{\rm NFW}(r)\, r^2\, dr, \tag{8}$$

which, considering Equation (7), renders

$$\int_0^{r_m} \rho_5(r)\, r^2\, dr = \int_0^{r_m} \rho_{\rm NFW}(r)\, r^2\, dr. \tag{9}$$

Examples of these cored DM profiles with NFW outskirts are given in Figure 6. This kind of piecewise shape has already been used in the literature, e.g., [29–31].

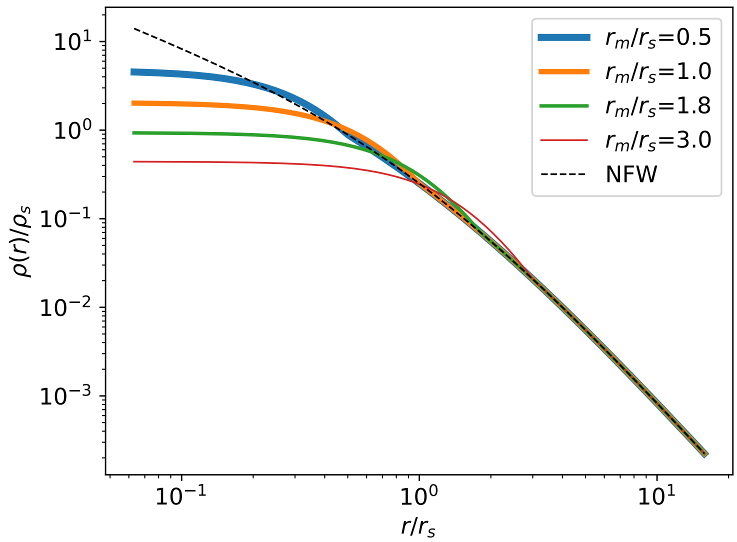

Figure 6. Piecewise density profiles with an inner core ($m = 5$ polytrope; ρ_5 in Equation (5)) and an outer NFW profile ($\rho_{\rm NFW}$; Equation (4)). The two pieces coincide at the matching radius r_m, $\rho_5(r_m) = \rho_{\rm NFW}(r_m)$, and the total mass is the total mass of $\rho_{\rm NFW}(r)$ (Equation (8)). The full NFW profile is shown as a black dashed line whereas profiles for different matching radii are shown with different colors as indicated in the inset.

Equations (7) and (9) provide a mapping between the parameters of the NFW profile (ρ_s and r_s) and the parameters defining the core (ρ_c and b). The continuity at r_m forces

$$\frac{\rho_c}{(1+(r_m/b)^2)^{5/2}} = \frac{\rho_s}{(r_m/r_s)(1+r_m/r_s)^2}, \tag{10}$$

whereas mass conservation, Equation (9), leads to

$$\rho_c\, r_m^3\, \frac{1}{3\,[1+(r_m/b)^2]^{3/2}} = \rho_s\, r_s^3 \left[\ln(1+\frac{r_m}{r_s}) - \frac{r_m/r_s}{1+r_m/r_s}\right]. \tag{11}$$

After some algrebra, Equations (10) and (11) render,

$$1 + \left(\frac{r_m/r_s}{b/r_s}\right)^2 = \frac{3\,(1+r_m/r_s)^2}{(r_m/r_s)^2} \left[\ln(1+\frac{r_m}{r_s}) - \frac{r_m/r_s}{1+r_m/r_s}\right], \tag{12}$$

and

$$\frac{\rho_c\, b^3}{\rho_s\, r_s^3} = \frac{3\,[1+(r_m/b)^2]^{3/2}}{(r_m/b)^3} \left[\ln(1+\frac{r_m}{r_s}) - \frac{r_m/r_s}{1+r_m/r_s}\right]. \tag{13}$$

We note that once r_m/r_s is set (i.e., the radius of match in units of r_s; see Equation (7)), Equations (12) and (13) give the full density profile. Equation (12) provides b/r_s, which can be used in Equation (13) to compute ρ_c/ρ_s, and then $\rho(r)/\rho_s$. This is the procedure followed to compute the densities shown in Figure 6.

Figure 7 shows the dependence on r_m/r_s for b/r_s, ρ_c/ρ_s, and $\rho_c b/(\rho_s r_s)$. We note that for $r_m \lesssim r_s$, $b \sim r_s$ and $\rho_c b \sim \rho_s r_s$. These dependences are easy to distill from the above equations in the limit $r_m \ll r_s$. In this case,

$$\ln(1 + \frac{r_m}{r_s}) - \frac{r_m/r_s}{1 + r_m/r_s} \simeq \frac{(r_m/r_s)^2}{2}, \tag{14}$$

so that Equation (12) renders,

$$b/r_s \simeq \sqrt{2}\,(r_m/r_s). \tag{15}$$

Similarly, Equation (13) plus Equation (15) render

$$\rho_c b \simeq \rho_s r_s\,(3/2)^2\sqrt{3} = \rho_s r_s \times 3.89711\ldots. \tag{16}$$

When $r_m = r_s$ (i.e., when the matching radius coincides with the characteristic radius defining the NFW profile), then things simplify even further so that

$$\frac{\rho_c r_c}{\rho_s r_s} \simeq 1.0068\ldots, \tag{17}$$

where we have used Equation (6) to transform b into r_c (details in Appendix B).

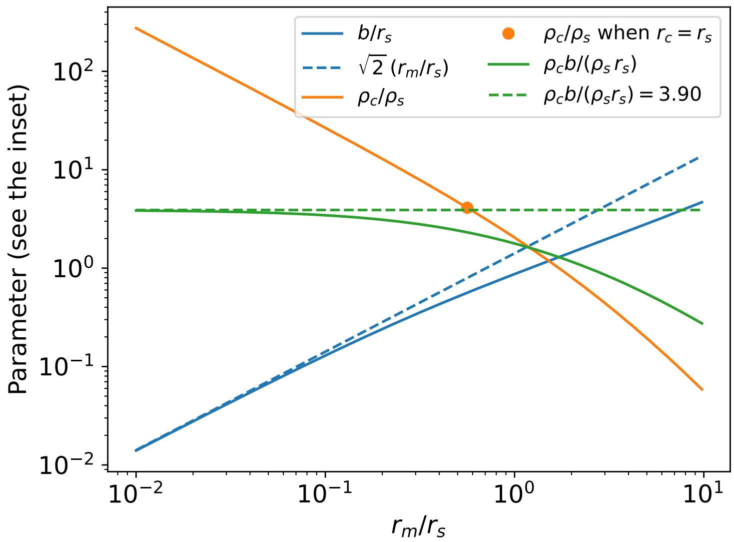

Figure 7. Dependence on r_m/r_s of b/r_s, ρ_c/ρ_s, and $\rho_c b/(\rho_s r_s)$ as given by Equations (12) and (13). The solid lines show the actual variation whereas the dashed lines correspond to the dependence when the transition radius $r_m \ll r_s$ (Equations (15) and (16)). The orange symbol points out when $r_c = r_s$, which has $r_m/r_s \simeq 0.56$ and $\rho_c/\rho_s \simeq 4.11$.

The NFW halos are given settings ρ_s and r_s. In the context of CDM, these two variables are often replaced by the concentration c and the halo mass M_h, so that

$$\rho_s = \frac{200\,c^3\,\rho_{crit}}{3\big[\ln(1+c) - c/(1+c)\big]}, \tag{18}$$

and

$$r_s^3 = \frac{3\,M_h}{800\pi\,\rho_{crit}\,c^3}. \tag{19}$$

The concentration c stands for r_{200}/r_s, with r_{200} defined so that the mean enclosed density within r_{200} equals 200 times the critical density ρ_{crit} of the Universe. Pieced together, Equations (18) and (19) render the dependence of the product $\rho_s r_s$ on c and M_h,

$$\rho_s r_s = \frac{10}{3}\left(\frac{30}{\pi}\right)^{1/3} \frac{\rho_{crit}^{2/3}\, c^2\, M_h^{1/3}}{\ln(1+c) - c/(1+c)}, \tag{20}$$

a relation that can be found already in the literature, e.g., [13].

The numerical simulations of CDM predict a relation between c and M_h, which varies with redshift and is quite tight for $M_h > 10^{10}\,M_\odot$ to become looser at smaller halo mass [32–34]. Examples of this relation are given in Figure 8, where we note that the range of variation of c is quite moderate, changing only by a factor of three for halos varying by seven orders of magnitude in mass, from 10^7 to $10^{14}\,M_\odot$; see the blue lines in Figure 8. Thus, considering c constant, the dependence of $\rho_s r_s$ on halo mass predicted by Equation (20) is quite mild as it scales as $M_h^{1/3}$. This fact, together with the approximate equivalence given by Equations (6) and (16), indicates that the predicted $\rho_c r_c$ is expected to vary little with halo mass,

$$\rho_c r_c \propto \rho_c b \propto \rho_s r_s \propto M_h^{1/3}, \tag{21}$$

as it is indeed observed (Section 2).

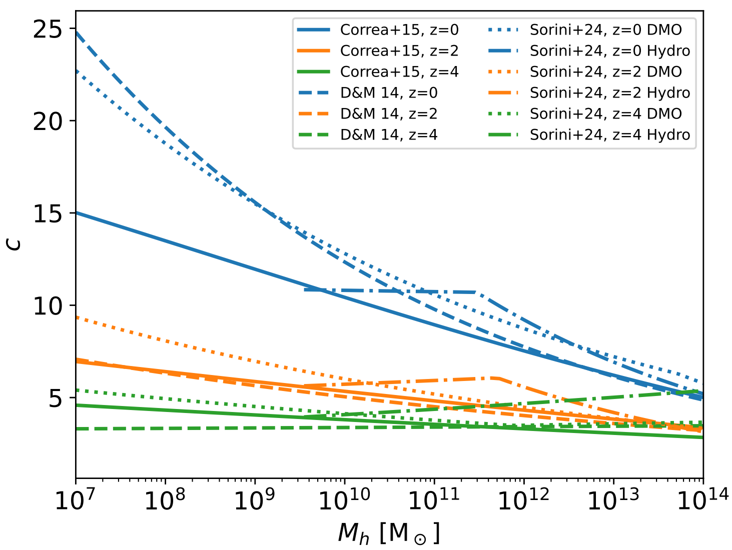

Figure 8. Relation between concentration c and halo mass M_h inferred from various CDM-only simulations. The three papers cited in the inset are D&M 14 [32], Correa+15 [33], and Sorini+24 [34]. For reference, we also show a relation obtained when baryon feedback is self-consistently treated in the simulation (the dotted dashed lines). Different redshifts (z) are included with different colors, whereas the type of line encodes the actual reference (see the inset).

The equations above yield $\rho_c r_c$ as a function of M_h. The algorithm to compute it is (1) set r_m/r_s, (2) obtain c of M_h from the literature (Figure 8), (3) obtain ρ_s and r_s as a function of M_h from Equations (18) and (19), (4) obtain b/r_s of M_h from r_s and Equation (12), (5) obtain ρ_c/ρ_s of M_h from b/r_s, r_m/r_s and Equation (13), (6) obtain r_c/b from Equation (6) and, finally, (7) compute

$$\rho_c r_c = \rho_s \times r_s \times \frac{b}{r_s} \times \frac{\rho_c}{\rho_s} \times \frac{r_c}{b}. \tag{22}$$

Figure 9 shows the predicted variation of $\rho_c r_c$ as a function of M_h for various r_m/r_s assuming the c–M_h relation at redshift zero given in [32] (the solid lines). Qualitatively, the trends for other c–M_h relations and redshifts look the same. The figure also includes the variation of r_c (the dashed lines) and ρ_c (the dashed dotted lines) separately. Note how the increase in r_c with M_h is partly balanced by the decrease in ρ_c, leaving a fairly constant $\rho_c r_c$.

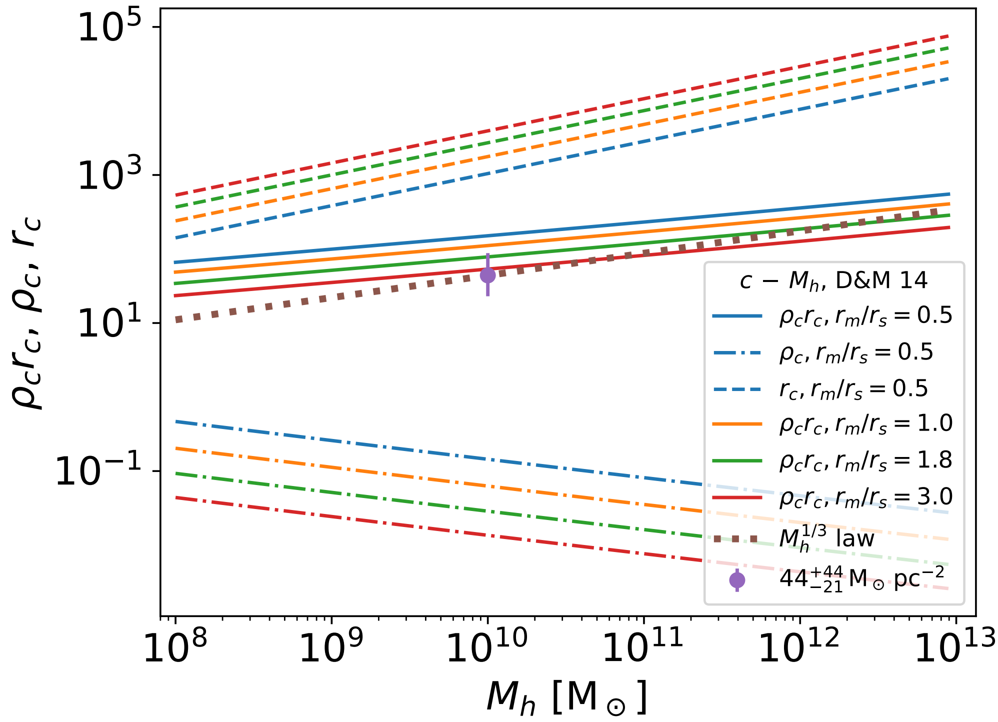

Figure 9. Predicted variation of the central mass surface density $\rho_c r_c$ as a function of M_h for various r_m/r_s assuming the c–M_h relation at redshift zero given in [32] (the solid lines). The figure also includes the variation of r_c (the dashed lines) and ρ_c (the dashed-dotted lines) to emphasize how the increase in r_c with increasing M_h is partly balanced by the decrease in ρ_c to produce a fairly constant $\rho_c r_c$. The dotted line shows the approximate dependence of $\rho_c r_c$ on M_h to be expected if c were constant (Equation (21)). This power law dependence has been anchored to the observed $\rho_c r_c$ (Equation (3)) assumed to represent $M_h \sim 10^{10}\,M_\odot$. The core density ρ_c and core radius r_c are given in units of $M_\odot$ pc^{-3} and pc, respectively.

4. Comparison Between Observations and Theory

Figure 10 shows the observed $\rho_c r_c$ (the symbols) compared with the prediction using the simple equations worked out in Section 3, where the DM cores are assumed to result from the redistribution of the mass of the CDM halos. The observed data points in Figure 10 are those in Figure 1 but shown in a range spanning the same eight orders of magnitude variation for both $\rho_c r_c$ and M_h. This particular scaling evidences how constant $\rho_c r_c$ is, with the range of values in Equation (3) highlighted as the pale green region. The colored lines represent the theoretical predictions and they agree well with the observation without any fine tuning. They even reproduce a slight increase in $\rho_c r_c$ with halo mass, which is probably too large in the theoretical model, although given the observational uncertainties one should not stress this fact further. Note that the prediction depends on the parameter r_m/r_s and the redshift z from which the relation c–M_h was taken. The best agreement with the observation corresponds to r_m/r_s between 1 and 2 starting off from halos at $z = 0$, and between 0.5 and 1 starting from halos a bit earlier at $z = 1$. Figure 10 is based on the theoretical c–M_h from [32], but the results are similar for the other theoretical c–M_h analyzed in Section 2 and Figures 8 and 9.

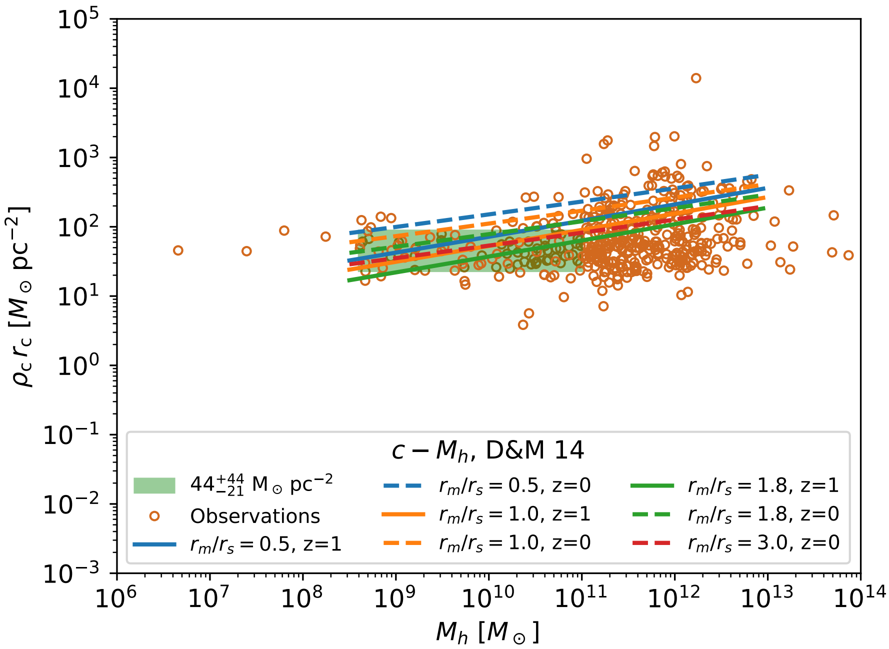

Figure 10. Observed versus predicted $\rho_c r_c$. The observations are the same as those used in Figure 1 except that ordinates and abscissae have been forced to span the same eight orders of magnitude range. The colored lines represent the theoretical predictions, which depend on the parameter r_m/r_s and the redshift z from which the c–M_h relation was taken (see the inset). The range of $\rho_c r_c$ values for $M_h < 10^{11}\,M_\odot$ given in Equation (3) is shown as the pale green region.

5. Discussion

Here, we analyze the implications of the fair agreement between the theory and observation presented in Section 4.

5.1. What Sets the c–M_h Relation?

Note that so far, the answer to the question of what sets $\rho_c r_c \simeq$ constant is *the existence of a c–M_h relation* for the DM halos produced in the ΛCDM cosmology (see Figures 8 and 9). Thus, unless we understand in physical terms what sets the c–M_h relation of the collisionless CDM halos, the above explanation of why $\rho_c r_c$ is constant sounds circular.

Correa et al. [33] describe the current understanding in detail, and give a number of relevant references. According to this view, the relation seems to be driven by the inside-out growth of the DM halos combined with the fact that low mass halos collapse first. The build-up of all halos generally consists of an early phase of fast accretion and a late phase where the accretion slows down [35,36]. During the early phase, halos are formed with low concentration, and then the concentration increases during the second phase as the outer halo grows and the mass accretion rate decreases. The concentration grows during this second phase because the virial radius setting the size of the whole halo increases while r_s remains rather constant. Halos of all masses undergo these two phases, but low mass halos complete the first phase early on and so they show large concentrations at present, whereas the very massive ones are still in the first phase. This process gives rise to the variation predicted by the numerical simulations shown in Figure 8. Contrary to the low mass halos, the high mass halos show little evolution of the concentration with redshift (or, equivalently, with time). According to this scenario, the actual c–M_h relation should depend significantly on the cosmological parameters, in particular, on σ_8 that parameterizes the amplitude of the matter density fluctuations in the early Universe, and on Ω_m that quantifies the total amount of matter. The larger σ_8 or Ω_m, the earlier the halos assemble and the larger the resulting concentration [33].

5.2. Relation Between DM Core Mass and Stellar Core Radius

The DM halo mass within the visible stellar core is

$$M_{hc} = \frac{4\pi}{3}\rho_c r_{\star c}^3 = \frac{4\pi g \kappa_c}{3}\, r_{\star c}^2, \tag{23}$$

with κ_c the constant $\rho_c r_c$, $r_{\star c}$ the stellar core radius, and $g = r_{\star c}/r_c$. Provided $g \lesssim 1$, Equation (23) gives the DM mass within the observed stellar core. Even if this is a relationship between the core DM halo mass and the stellar radius, it is encouraging to note that a similar relation is observed to hold between the DM core mass and the DM core radius (Figure 4), and between the total DM halo mass and the core radius; see the dashed line in Figure 5, corresponding to $M_h \propto r_c^{2.5}$. The baryon fraction in the core, defined as

$$f_{bc} = \frac{M_{\star c}}{M_{hc}} = \frac{\rho_{\star c} r_{\star c}}{g\kappa_c}, \tag{24}$$

can be inferred from the observed stellar mass surface density, $\rho_{\star c} r_{\star c}$, provided g can be measured or estimated. Thus, if Equation (1) holds, from the stellar distribution alone one can estimate the DM core mass and the baryon fraction in the core. Using κ_c from Equation (3), Equations (23) and (24) become

$$M_{hc} \simeq 1.7^{+1.7}_{-0.8} \times 10^5\, M_\odot \left(\frac{r_{\star c}}{30\,\mathrm{pc}}\right)^2 g, \tag{25}$$

and

$$f_{bc} \simeq 2.2^{+2.1}_{-1.1} \times 10^{-3}\, \frac{\rho_{\star c} r_{\star c}}{0.1\, M_\odot\,\mathrm{pc}^{-2}}\, g^{-1}, \tag{26}$$

respectively. The error bars just consider the scatter in κ_c.

In order to test the reliability of the above equations, we have used existing observations of ultra faint dwarfs (UFDs) and dwarf spheroidal galaxies (dSph) to compare for individual galaxies the values of M_{hc} computed from velocities and from Equation (25). The dynamical mass of a galaxy within $r_{\star c}$ can be computed from the observed velocity dispersion within the core radius, $\sigma_{\star c}$, as

$$M_{dyn} = \frac{2\ln 2}{G}\sigma_{\star c}^2\, r_{\star c}, \tag{27}$$

with G being the gravitational constant. In DM-dominated systems,

$$M_{hc} \simeq M_{dyn}. \tag{28}$$

Equation (27) uses the definition in Equation (2) and assumes spherical symmetry as detailed by, e.g., [11]. It differs from similar expressions found in the literature by factors of the order of one [37]. Figure 11 shows the DM halo mass estimated from photometry (Equation (25)) versus the value estimated from velocity dispersion (Equations (27) and (28)). The agreement is quite remarkable; often within the error bars set by Equation (3). The UFDs have been included to show that the approximation works even in this extremely low mass regime, keeping in mind that part of the observed scatter away from the one-to-one relation is due to uncertainties in their dynamical mass estimate. The dynamical masses of UFDs are particularly uncertain because they are affected by the presence of stellar binaries, which may contribute to the velocity dispersion as much as the gravitational potential, e.g., [38]. The horizontal error bars in Figure 11 result from the statistical errors in $\sigma_{\star c}$, which are probably underestimating the real ones since the effect of the binaries is not included. We have used $g = 1$ for simplicity but the assumption $g \sim 1$ seems to be quite realistic [25,26] and, eventually, it could be relaxed and refined if needed.

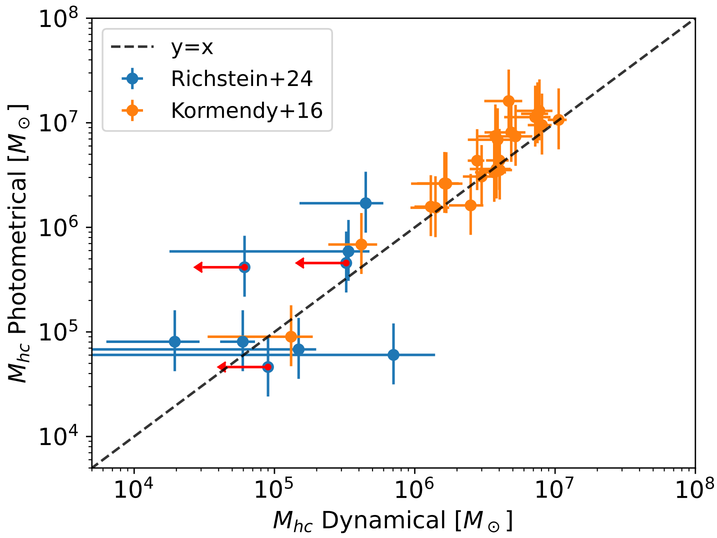

Figure 11. Comparison between the DM halo mass in the core of galaxies computed from the stellar velocity dispersion (horizontal axis) and from photometry alone as described by Equation (25) (vertical axis). The represented points include UFDs from Richstein+24 [37] and dSphs from Kormendy+16 [11]. The vertical error bars represent the dispersion in $\rho_c r_c$ (Equation (3)) whereas the horizontal error bars account for the uncertainties in $\sigma_{\star c}$, as quoted in the original references. The one-to-one line is shown as a dashed black line. The red arrows point out upper limits in the dynamical DM halo masses.

Given the good agreement between the dynamical DM mass and the photometric DM mass represented in Figure 11, Equation (25) seems to be a new valuable tool for estimating the DM halo mass from photometry alone. Photometry is much cheaper observationally than the spectroscopy required to determine the dynamical mass. The validity of Equation (25) implies the validity of Equation (26), which also provides a new empirical way of estimating the baryon fraction in galaxies only from stellar photometry. Moreover, it tells us that the surface density of stars is a proxy for the baryon fraction in the inner parts of a galaxy.

The above estimate can be extended to the mass of the whole DM halo using a model to represent the DM halo beyond the core (e.g., the piecewise profile in Equation (7) and Figure 6). Thus, M_{hc} can be used to estimate M_h. To have a first idea of the ratio between them, assume that the stellar core radius is not very different from the matching radius r_m that separates the inner and outer parts of the piecewise profile (Figure 6), which is a quite common assumption in the literature, e.g., [13,39]. Then, the ratio of masses turns out to be

$$M_h/M_{hc} \simeq \frac{\ln(1+r_{\star c}/r_s) - (r_{\star c}/r_s)/(1+r_{\star c}/r_s)}{\ln(1+c) - c/(1+c)}, \tag{29}$$

which varies from a few to a factor of ten when the concentration varies as predicted, from $c \sim 5$ in high mass halos to $c \sim 20$ in low mass halos (Figure 8, the blue lines).

5.3. Constant DM Dynamical Pressure

The dynamical pressure in a fluid scales like the density times the square of the characteristic velocity. Thus, for the DM in the core, the effective DM dynamical pressure is

$$P_c \propto \rho_c \sigma_c^2, \tag{30}$$

with σ_c being the velocity dispersion of the DM particles in the core. Assuming the DM cores are to be virialized (i.e., assuming that Equations (27) and (28) hold for the DM particles too), then

$$P_c \propto (\rho_c\, r_c)^2 \simeq \text{constant}, \tag{31}$$

so that Equation (1) implies that the dynamical pressure to be exerted by the DM particles if they could collide would be the same in all halos, independently of their total mass or size. However, collisionless CDM particles do not collide, and Equation (31) has to be interpreted as a property that emerges from the existence of the c–M_h relation.

6. Conclusions

We reviewed the observational evidence for $\rho_c r_c \simeq$ constant (Equation (1); Section 2) and then put forward a simple version of the commonly accepted interpretation behind it (Section 3). Equation (1) requires the existence of a core in the DM distribution. Halos formed in DM-only CDM cosmological numerical simulations do not have inner cores but cusps (Equation (4)); however, if any physical process redistributes the DM particles of the expected CDM halos, then Equation (1) is satisfied automatically. It emerges from the relation between the concentration and DM halo mass expected in ΛCDM cosmological simulations. This relation is set by the time of halo formation, so that low mass halos form earlier and present larger concentrations (Section 5.1). The conventional explanation to understand how the original cuspy CDM halos become cored halos is stellar feedback. This term encapsulates all the baryon-driven processes that shuffle gas and mass around (e.g., supernova explosions or stellar winds), modifying the overall potential, including the distribution of DM particles in the center of the galaxies [18,19]. However, this transformation is not specific to stellar feedback, keeping in mind that any physical process that thermalizes a self-gravitating structure tends to form cores [21,22]. Thus, any other sensible physical process that redistributes matter without altering the original mass of the CDM halos is able to account for Equation (1). In other words, the property of $\rho_c r_c$ to be approximately constant is not specific to CDM but, rather, it is also expected in many alternative DM theories forming cores, e.g., [13,31,40]. Theories that only redistribute mass to produce cores have the advantage of leaving the large scale structure of the Universe unchanged, thus being in agreement with the standard ΛCDM.

The mathematical development in Section 3 parallels others existing in the literature, except that the core is modeled with a different expression, e.g., [13,15]. Here, we provide a full account of the derivation of the main equations for the sake of comprehensiveness, which help us to make the qualitative comparison with observations in Section 4. However, we could have started off by assuming the relevant Equations (12) and (13) and proceed from here. This loose dependence of the results on the actual shape of the core is consistent with the fact that other alternative forms of the piecewise profile with cores that we tried (top hat profiles) render qualitatively similar results.

The agreement between the simple theory and observations is notable, keeping in mind that there is no fitting or fine tuning in matching lines and points in Figure 10. Even more, the theory predicts a moderate increase in $\rho_c r_c$ with M_h, similarly to the one hinted at by the observations. However, the best fitting c–M_h relations correspond to large cores (the green dashed line represents $r_m/r_s = 1.8$) or $z \neq 0$ (the solid orange and green lines in Figure 10 correspond to $z = 1$). The latter is a result that we do not understand; even if the transformation of cusps to cores requires time and starts at high redshift, the accretion of DM in the outskirts of the halos should continue all the way to the present, a process leading to the c–M_h relation at $z = 0$. As we discussed in Section 5.1, the c–M_h depends on the cosmological parameters σ_8 and Ω_m since they set the assembly time of the DM halos. Varying them may improve the agreement when employing the theoretical c–M_h relations at $z = 0$, but we have not pursued this idea further.

As a byproduct of the effort to compile $\rho_c r_c$ values, we show that the fact that the product is constant can be used to estimate the mass in the DM halo of a galaxy from the distribution of stars alone. This possibility can be very useful for low stellar mass galaxies where the determination of their DM content using traditional kinematical measurements is technically difficult, whereas their photometry is doable. The same argument allows one to estimate the baryon fraction in the core of these systems. Dwarf galaxies also tend to show a core in the stellar distribution, e.g., [23,24], with the radii of the stellar and DM cores expected to scale with each other [25,26]. This idea plus Equation (3) allows us to propose specific relations between the observed stellar core radius and the DM core mass (Equation (25)) and between the observed stellar mass surface density and the baryon fraction in the core (Equation (26)). The latter tells us that the surface density of stars is a proxy for the baryon fraction in the inner parts of a galaxy. The proposed calibrations are in good agreement with DM masses estimated from dynamical measurements in low mass galaxies (Figure 11). Note that the numerical coefficients of the proposed scaling laws depend on the definition of the core radius, for which we adopted Equation (2). Other definitions can be trivially recalibrated.

Funding: This research has been partly funded through grant PID2022-136598NB-C31 (ESTALLIDOS8) by MCIN/AEI/10.13039/501100011033 and by "ERDF A way of making Europe". It was also supported by the European Union through the grant "UNDARK" of the widening participation and spreading excellence programme (project number 101159929).

Data Availability Statement: All the data used in this paper are publicly available in the cited references.

Acknowledgments: I am grateful to Ignacio Trujillo for bringing to my attention the empirical relationship explored in the work (Equation (1)). I am also thankful to him, Claudio Dalla Vecchia, Angel Ricardo Plastino, Camila Correa, and Andrés Balaguera for enlightening discussions and clarifications on various issues addressed in the manuscript.

Conflicts of Interest: The author declares no conflicts of interest.

Abbreviations

The following abbreviations are used in this manuscript:

DM	Dark matter
CDM	Cold dark matter
dSph	Dwarf spheroidal galaxy
ΛCDM	Concordance cosmological model
UFD	Ultra faint dwarf

Appendix A. Bibliography on the $\rho_c r_c$ Versus M_h Relation

This appendix details the use of the bibliography leading to Figures A1, 1, 3–5 and 10. Since the estimate of the parameters is cumbersome, we discuss the main issues and assumptions in this appendix and in Table A1. The various references are identified in the figures through the corresponding insets.

- Burkert (1995) [4] explicitly gives a relation between the central density and core radius and between the halo mass and core radius. Pieced together, they provide the relation represented in Figure 1 with M_h within the range represented in his Figure 3. The original relations have to be corrected to our core radius definition (Equation (2)) and to the total halo mass (his Equation (4)).
- Donato et al. (2009) [7]. The value with error bars is directly given in the paper. They conclude that the product $\rho_c r_c$ is constant for absolute magnitudes M_B from -7 to -22. In order to transform these B magnitudes into halo masses, (1) we use a stellar mass-to-light ratio $M_\star/L_\star$ of one (in solar units) and then use $M_\star$ to estimate M_h using the halo to stellar mass ratio at redshift zero from [27]. They use the same definition of the core radius as [4], and so it has to be corrected to ours in Equation (2).

- Burkert (2015) [10]. We take ρ_c and r_c from [10], and the corresponding $M_\star$ from [41]. Then M_h was estimated using the halo to stellar mass ratio from [27]. The conversion between the core radius used in the original work and Equation (2) was carried out based on Figure 1 of [10].
- Oh et al. (2015) [2] do not determine the product $\rho_c r_c$, but they provide ρ_c and r_c separately. They also provide the absolute V magnitude M_V which, assuming a mass-to-light ratio of one, allows us to estimate M_h using the DM halo to stellar mass ratio from [27]. The r_c used in this reference happens to agree with Equation (2) and so we do not change it. The averages in Table A1 were computed after removing the $\rho_c r_c$ values with a larger error (see Figure 1).
- Kormendy and Freeman (2016) [11] is the reference with the largest number of galaxies. It gives clear relations between ρ_c and r_c, and M_B. The galaxies are separated into low and high masses. As for many of the above references, M_h is obtained from their M_B assuming a stellar mass-to-light ratio of one and using the scaling between stellar and halo mass in [27]. For the core radius, the authors directly provide the scaling between their core radius and Equation (2).
- Spano et al. (2008) [6] also find approximately constant $\rho_c r_c$. The galaxies are fairly massive (see Table A1). No error bars are given. We transform their r_s into ours.
- Saburova and Del Popolo (2014) [9] compile a large list of objects from various sources. The authors compute and provide the product $\rho_c r_c$. We infer M_h from M_B as explained above. The points without error bars in Figure 1 are not points with zero error but points without an estimate of the error. They claim a variation with luminosity so that the more luminous (and so more massive) galaxies have larger $\rho_s r_s$ (see Figure 1). The low mass value is consistent with other estimates. They use a Burkert DM halo to define the radius, which we transform to our definition in Equation (2).
- Salucci et al. (2012) [8]. We consider only the data for the dwarf spheroidal galaxies (dSph).
- Di Paolo et al. (2019) [12]. These are low surface brightness galaxies, but seem to behave as the rest. Galaxies are stacked in halo mass bins. We take the halo mass from them and then correct r_c to accommodate their definition (Burkert profile) into our definition (Equation (2)).

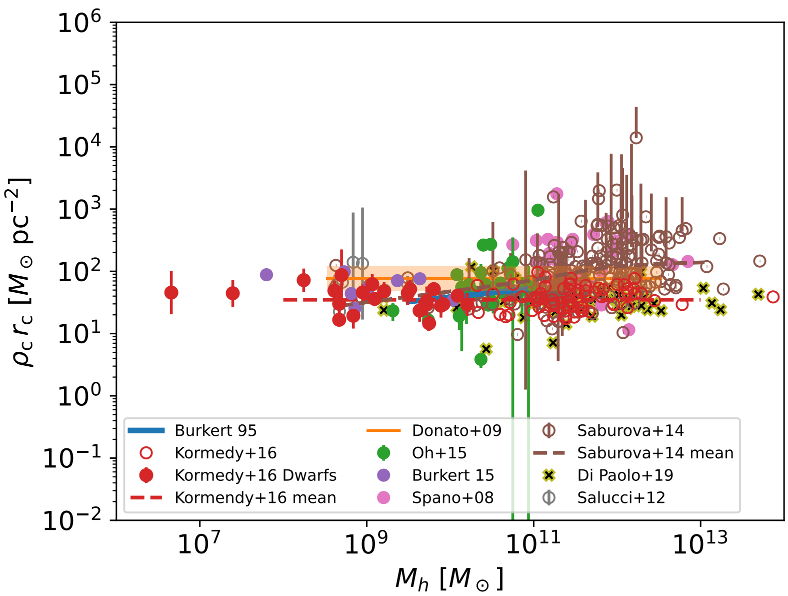

Figure A1. Figure identical to Figure 1 except that the range of the ordinates ($\rho_c r_c$) has been expanded to show the same eight orders of magnitude variation as the DM halo mass range (M_h). For the rest of details, see Figure 1.

Table A1. References used to constraint $\rho_c r_c$.

Reference	$\rho_c r_c$ $[M_\odot \, \mathrm{pc}^{-2}]$ [1]	$\log M_h$ $[M_\odot]$ [2]	Comment [3]
[4] Burkert (1995)	41.5 ± 5.9	10.2 ± 0.4	Corrected r_c & M_h
[7] Donato et al. (2009)	76^{+43}_{-16}	8.5–12.5	Corrected r_c; M_h from M_B
[10] Burkert (2015)	64^{+56}_{-34}	9.0 ± 0.6	Corrected r_c
[2] Oh et al. (2015)	67 ± 65	10.4 ± 0.4	Sigma-clipping in noise
[11] Kormendy and Freeman (2016)	39 ± 17	11.5 ± 0.6	Massive galaxies. Corrected r_c
[11] Kormendy and Freeman (2016)	40 ± 17	9.1 ± 0.8	Dwarfs. Corrected r_c
[6] Spano et al. (2008)	230 ± 300	11.5 ± 0.5	Corrected r_c
[9] Saburova and Del Popolo (2014)	59 ± 36	8.6–11	Only low mass. Corrected r_c.
[8] Salucci et al., 2012	71 ± 40	9.0 ± 0.4	dSph only. Corrected r_c
[12] Di Paolo et al., 2019	41 ± 21	9.2–13.7	Corrected r_c, using their M_h.

[1] Mean and standard deviation of the values mentioned in the reference. [2] Mean and standard deviation or range of values. [3] Further details given in Appendix A.

Appendix B. The Theoretical Value of $\rho_c r_c$ When $r_m = r_s$

In the case when the matching radius of the piecewise profile is equal to the characteristic radius of the corresponding NFW profile ($r_m/r_s = 1$ in Figure 6), several numerical coincidences happen and $\rho_c r_c$ and $\rho_s r_s$ are almost equal,

$$\frac{\rho_c r_c}{\rho_s r_s} = \frac{8[3(\ln 2 - 1/2)]^{5/2}\,[2^{2/5} - 1]^{1/2}}{[12(\ln 2 - 1/2) - 1]^{1/2}} \simeq 1.0068\ldots. \tag{A1}$$

It follows from Equations (6), (12) and (13) when $r_m = r_s$.

References

1. Persic, M.; Salucci, P.; Stel, F. The universal rotation curve of spiral galaxies—I. The dark matter connection. *Mon. Not. R. Astron. Soc.* **1996**, *281*, 27–47. [CrossRef]
2. Oh, S.H.; Hunter, D.A.; Brinks, E.; Elmegreen, B.G.; Schruba, A.; Walter, F.; Rupen, M.P.; Young, L.M.; Simpson, C.E.; Johnson, M.C.; et al. High-resolution Mass Models of Dwarf Galaxies from LITTLE THINGS. *Astron. J.* **2015**, *149*, 180. [CrossRef]
3. Salucci, P. The distribution of dark matter in galaxies. *Astron. Astrophys. Rev.* **2019**, *27*, 2. [CrossRef]
4. Burkert, A. The Structure of Dark Matter Halos in Dwarf Galaxies. *Astrophys. J.* **1995**, *447*, L25–L28. [CrossRef]
5. Salucci, P.; Burkert, A. Dark Matter Scaling Relations. *Astrophys. J.* **2000**, *537*, L9–L12. [CrossRef]
6. Spano, M.; Marcelin, M.; Amram, P.; Carignan, C.; Epinat, B.; Hernandez, O. GHASP: An Hα kinematic survey of spiral and irregular galaxies—V. Dark matter distribution in 36 nearby spiral galaxies. *Mon. Not. R. Astron. Soc.* **2008**, *383*, 297–316. [CrossRef]
7. Donato, F.; Gentile, G.; Salucci, P.; Frigerio Martins, C.; Wilkinson, M.I.; Gilmore, G.; Grebel, E.K.; Koch, A.; Wyse, R. A constant dark matter halo surface density in galaxies. *Mon. Not. R. Astron. Soc.* **2009**, *397*, 1169–1176. [CrossRef]
8. Salucci, P.; Wilkinson, M.I.; Walker, M.G.; Gilmore, G.F.; Grebel, E.K.; Koch, A.; Frigerio Martins, C.; Wyse, R.F.G. Dwarf spheroidal galaxy kinematics and spiral galaxy scaling laws. *Mon. Not. R. Astron. Soc.* **2012**, *420*, 2034–2041. [CrossRef]
9. Saburova, A.; Del Popolo, A. On the surface density of dark matter haloes. *Mon. Not. R. Astron. Soc.* **2014**, *445*, 3512–3524. [CrossRef]
10. Burkert, A. The Structure and Dark Halo Core Properties of Dwarf Spheroidal Galaxies. *Astrophys. J.* **2015**, *808*, 158. [CrossRef]
11. Kormendy, J.; Freeman, K.C. Scaling Laws for Dark Matter Halos in Late-type and Dwarf Spheroidal Galaxies. *Astrophys. J.* **2016**, *817*, 84. [CrossRef]
12. Di Paolo, C.; Salucci, P.; Erkurt, A. The universal rotation curve of low surface brightness galaxies—IV. The interrelation between dark and luminous matter. *Mon. Not. R. Astron. Soc.* **2019**, *490*, 5451–5477. [CrossRef]
13. Lin, H.W.; Loeb, A. Scaling relations of halo cores for self-interacting dark matter. *J. Cosmol. Astropart. Phys.* **2016**, *2016*, 009. [CrossRef]
14. Burkert, A. Fuzzy Dark Matter and Dark Matter Halo Cores. *Astrophys. J.* **2020**, *904*, 161. [CrossRef]
15. Kaneda, Y.; Mori, M.; Otaki, K. A universal scaling relation incorporating the cusp-to-core transition of dark matter halos. *Publ. Astron. Soc. Jpn.* **2024**, *76*, 1026–1040. [CrossRef]
16. Navarro, J.F.; Frenk, C.S.; White, S.D.M. A Universal Density Profile from Hierarchical Clustering. *Astrophys. J.* **1997**, *490*, 493–508. [CrossRef]

17. Wang, J.; Bose, S.; Frenk, C.S.; Gao, L.; Jenkins, A.; Springel, V.; White, S.D.M. Universal structure of dark matter haloes over a mass range of 20 orders of magnitude. *Nature* **2020**, *585*, 39–42. [CrossRef] [PubMed]
18. Governato, F.; Brook, C.; Mayer, L.; Brooks, A.; Rhee, G.; Wadsley, J.; Jonsson, P.; Willman, B.; Stinson, G.; Quinn, T.; et al. Bulgeless dwarf galaxies and dark matter cores from supernova-driven outflows. *Nature* **2010**, *463*, 203–206. [CrossRef]
19. Pontzen, A.; Governato, F. Cold dark matter heats up. *Nature* **2014**, *506*, 171–178. [CrossRef]
20. Lazar, A.; Bullock, J.S.; Boylan-Kolchin, M.; Chan, T.K.; Hopkins, P.F.; Graus, A.S.; Wetzel, A.; El-Badry, K.; Wheeler, C.; Straight, M.C.; et al. A dark matter profile to model diverse feedback-induced core sizes of ΛCDM haloes. *Mon. Not. R. Astron. Soc.* **2020**, *497*, 2393–2417. [CrossRef]
21. Plastino, A.R.; Plastino, A. Stellar polytropes and Tsallis' entropy. *Phys. Lett. A* **1993**, *174*, 384–386. [CrossRef]
22. Sánchez Almeida, J.; Trujillo, I.; Plastino, A.R. The principle of maximum entropy explains the cores observed in the mass distribution of dwarf galaxies. *Astron. Astrophys.* **2020**, *642*, L14. [CrossRef]
23. Carlsten, S.G.; Greene, J.E.; Greco, J.P.; Beaton, R.L.; Kado-Fong, E. Structures of Dwarf Satellites of Milky Way-like Galaxies: Morphology, Scaling Relations, and Intrinsic Shapes. *Astrophys. J.* **2021**, *922*, 267. [CrossRef]
24. Montes, M.; Trujillo, I.; Karunakaran, A.; Infante-Sainz, R.; Spekkens, K.; Golini, G.; Beasley, M.; Cebrián, M.; Chamba, N.; D'Onofrio, M.; et al. An almost dark galaxy with the mass of the Small Magellanic Cloud. *Astron. Astrophys.* **2024**, *681*, A15. [CrossRef]
25. Sánchez Almeida, J.; Trujillo, I.; Plastino, A.R. The Stellar Distribution in Ultrafaint Dwarf Galaxies Suggests Deviations from the Collisionless Cold Dark Matter Paradigm. *Astrophys. J.* **2024**, *973*, L15. [CrossRef]
26. Sánchez Almeida, J.; Trujillo, I.; Montes, M.; Plastino, A.R. Constraining the shape of dark matter haloes using only starlight: I. A new technique and its application to the galaxy Nube. *Astron. Astrophys.* 2024, *submitted*.
27. Behroozi, P.S.; Wechsler, R.H.; Conroy, C. The Average Star Formation Histories of Galaxies in Dark Matter Halos from z = 0-8. *Astrophys. J.* **2013**, *770*, 57. [CrossRef]
28. Sánchez Almeida, J. The Principle of Maximum Entropy and the Distribution of Mass in Galaxies. *Universe* **2022**, *8*, 214. [CrossRef]
29. Robertson, A.; Massey, R.; Eke, V.; Schaye, J.; Theuns, T. The surprising accuracy of isothermal Jeans modelling of self-interacting dark matter density profiles. *Mon. Not. R. Astron. Soc.* **2021**, *501*, 4610–4634. [CrossRef]
30. Sánchez Almeida, J.; Trujillo, I. Numerical simulations of dark matter haloes produce polytropic central cores when reaching thermodynamic equilibrium. *Mon. Not. R. Astron. Soc.* **2021**, *504*, 2832–2840. [CrossRef]
31. Kaplinghat, M.; Tulin, S.; Yu, H.B. Dark Matter Halos as Particle Colliders: Unified Solution to Small-Scale Structure Puzzles from Dwarfs to Clusters. *Phys. Rev. Lett.* **2016**, *116*, 041302. [CrossRef]
32. Dutton, A.A.; Macciò, A.V. Cold dark matter haloes in the Planck era: Evolution of structural parameters for Einasto and NFW profiles. *Mon. Not. R. Astron. Soc.* **2014**, *441*, 3359–3374. [CrossRef]
33. Correa, C.A.; Wyithe, J.S.B.; Schaye, J.; Duffy, A.R. The accretion history of dark matter haloes - III. A physical model for the concentration-mass relation. *Mon. Not. R. Astron. Soc.* **2015**, *452*, 1217–1232. [CrossRef]
34. Sorini, D.; Bose, S.; Pakmor, R.; Hernquist, L.; Springel, V.; Hadzhiyska, B.; Hernández-Aguayo, C.; Kannan, R. The impact of baryons on the internal structure of dark matter haloes from dwarf galaxies to superclusters in the redshift range $0 < z < 7$. *arXiv* **2024**, arXiv:2409.01758. [CrossRef]
35. Zhao, D.H.; Mo, H.J.; Jing, Y.P.; Börner, G. The growth and structure of dark matter haloes. *Mon. Not. R. Astron. Soc.* **2003**, *339*, 12–24. [CrossRef]
36. Lu, Y.; Mo, H.J.; Katz, N.; Weinberg, M.D. On the origin of cold dark matter halo density profiles. *Mon. Not. R. Astron. Soc.* **2006**, *368*, 1931–1940. [CrossRef]
37. Richstein, H.; Kallivayalil, N.; Simon, J.D.; Garling, C.T.; Wetzel, A.; Warfield, J.T.; van der Marel, R.P.; Jeon, M.; Rose, J.C.; Torrey, P.; et al. Deep Hubble Space Telescope Photometry of Large Magellanic Cloud and Milky Way Ultrafaint Dwarfs: A Careful Look into the Magnitude–Size Relation. *Astrophys. J.* **2024**, *967*, 72. [CrossRef]
38. Pianta, C.; Capuzzo-Dolcetta, R.; Carraro, G. The Impact of Binaries on the Dynamical Mass Estimate of Dwarf Galaxies. *Astrophys. J.* **2022**, *939*, 3. [CrossRef]
39. Outmezguine, N.J.; Boddy, K.K.; Gad-Nasr, S.; Kaplinghat, M.; Sagunski, L. Universal gravothermal evolution of isolated self-interacting dark matter halos for velocity-dependent cross-sections. *Mon. Not. R. Astron. Soc.* **2023**, *523*, 4786–4800. [CrossRef]
40. Correa, C.A.; Schaller, M.; Ploeckinger, S.; Anau Montel, N.; Weniger, C.; Ando, S. TangoSIDM: Tantalizing models of self-interacting dark matter. *Mon. Not. R. Astron. Soc.* **2022**, *517*, 3045–3063. [CrossRef]
41. McConnachie, A.W. The Observed Properties of Dwarf Galaxies in and around the Local Group. *Astron. J.* **2012**, *144*, 4. [CrossRef]

Disclaimer/Publisher's Note: The statements, opinions and data contained in all publications are solely those of the individual author(s) and contributor(s) and not of MDPI and/or the editor(s). MDPI and/or the editor(s) disclaim responsibility for any injury to people or property resulting from any ideas, methods, instructions or products referred to in the content.